IEEE Access
Multidisciplinary | Rapid Review | Open Access Journal

IEEE MAGNETICS SOCIETY SECTION

Received 14 March 2023, accepted 30 March 2023, date of publication 5 April 2023, date of current version 11 April 2023.

*Digital Object Identifier 10.1109/ACCESS.2023.3264871*

RESEARCH ARTICLE

# Expansion of Motor High-Efficiency Area by Inserting Magnetic Composite Material into Rotor

**MITSUHIDE SATO[1], (Member, IEEE), KEIGO TAKAZAWA[1], RYO YOSHIDA[1], MASAMI NIREI[2], (Member, IEEE), AND TSUTOMU MIZUNO[1], (Senior Member, IEEE)**

[1]Faculty of Engineering, Shinshu University, Nagano 380-8553, Japan
[2]National Institute of Technology, Nagano College, Nagano 381-8550, Japan

Corresponding author: Mitsuhide Sato (mitsuhide@shinshu-u.ac.jp)

This work was supported in part by the New Energy and Industrial Technology Development Organization (NEDO), in part by Research Grant Technova Inc., and in part by the Tsugawa Foundation.

**ABSTRACT** Variable magnetic flux motors have been proposed to achieve high-efficiency operation over a wide drive range ranging from high torque to high-speed. This paper clarifies the high efficiency area expansion effect of a variable flux motor with a magnetic composite material inserted in the rotor. To achieve the effect of enlarging the maximum efficiency range, this motor uses magnetic composite materials with much lower saturation magnetic flux density and iron loss than electromagnetic steel plate. This paper reports the magnetic and mechanical properties of the magnetic composite material using Fe–Si–Al alloy, considering low iron loss. The simulation results clarified the variable magnetic flux characteristics for reducing loss at high-speed rotation by actively utilizing the magnetic saturation region of the magnetic composite material. The efficiency improvement in the high-speed region is attributed to the suppression of spatial harmonics without significantly reducing the q-axis inductance. Furthermore, the proposed motor achieves both the expansion of the high-efficiency range and relaxation of mechanical stress by increasing the thickness of the bridge part adjacent to the permanent magnet.

**INDEX TERMS** Field-weakening control, magnetic composite material, spatial harmonics, variable magnetic flux motor.

## I. INTRODUCTION

The high-efficiency of electric motors used in a wide range of fields is indispensable for preventing global warming [1], [2], [3], [4]. The progress of electrification of propulsion motors for automobiles and aircraft will increase the demand for higher efficiency over a wide operating range [5], [6], [7], [8], [9], [10].

An interior permanent magnet synchronous (IPM) motor with a structure in which a permanent magnet is embedded inside the rotor is effective for improving efficiency [11], [12]. The IPM motor's weakened field current control allows for a wide operating range from low- to high-speed rotation [13], [14], [15]. Furthermore, by utilizing reluctance torque, the field weakening current is effective in improving torque performance. The weakened field current in the high-speed rotation region lowers the counter electromotive force constant, allowing the operating region to be expanded, but it tends to increase copper and iron losses.

Variable magnetic flux motors have been proposed to realize high-efficiency operation in a wide drive range from high torque to high-speed range [16], [17], [18], [19], [20], [21]. The variable torque constant is achieved by controlling the amount of field magnetic flux from the outside. A combination of low coercive magnets in the high coercive magnet vicinity of the rotor also realizes variable field magnetism [22], [23], [24], [25]. The low-coercivity magnet shape and rotor insertion position determine the high-efficiency range of the variable magnetic field motor [26]. A parallel-inserted hybrid permanent magnet motor has been proposed, with high efficiency, high speed, and a wide magnetization adjustment range [27]. Additionally, permanent magnets have been

The associate editor coordinating the review of this manuscript and approving it for publication was Valentine Novosad.

engineered to realize variable magnetic fields [28], [29]. Furthermore, an axial motor for in-wheel motors has been proposed that controls the magnetization state of thermosetting resin with a field winding to change the field magnetic flux [30]. The stator coil's pulse current modifies the magnetic force of the low magnetic force magnet, which controls the magnetic flux. Mechanically varying to realize a variable magnetic flux has been proposed [31]. Variable flux motors with stator windings that cause magnetic saturation of the electromagnetic steel plate via a three-dimensional magnetic path have also been proposed [32]. These motors, however, necessitate an increase in inverter capacity, the addition of coils and actuators, and complicate the mechanism. As a result, a simple structure with variable magnetic flux is required.

A variable leakage flux (VLF) motor that can obtain the effect of variable flux only by vector control used in general motors has been proposed [33]. This motor has a flux barrier in the rotor core that is shaped to take into account the armature reaction from the stator. Controlling the magnitude and phase of the armature current for the magnetic flux interlinking from the permanent magnet to the coil results in variable magnetic flux. The magnetic flux of the magnet is short-circuited in the rotor, which causes a decrease in the interlinkage magnetic flux to the armature in the high-speed rotation and low torque region. This phenomenon realizes the suppression of the field weakening current caused by a decrease in the counter electromotive force constant [33]. Due to magnetic flux saturation, VLF motors have large variable salient pole characteristics, making it difficult to estimate the rotor position with high precision. Real-time acquisition of motor parameters enables a sensorless control of VLF motors that accounts for magnetic flux saturation [34], [35].

This paper examines the performance of variable flux motors utilizing magnetic composites (abbreviated as MC motors). Magnetic composite material is created by combining magnetic powder and resin and sintering it [36], [37], [38], [39], [40]. This material has a unique magnetic property that the saturation magnetic flux density and magnetic permeability can be easily controlled by changing the type of the magnetic powder. The loss of a high-speed rotary motor is primarily affected by spatial harmonics caused by the magnetic flux's large time fluctuation. The use of magnetic composite material with precisely controlled permeability in the stator is effective in lowering the spatial harmonics of high-speed rotary motors [41], [42].

The MC motor obtains variable magnetic flux characteristics by using the magnetic flux saturation of the magnetic composite material. The magnetic composite material is introduced into the rotor flux barrier, which has been magnetically saturated by the stator's armature reaction. The variable magnetic flux due to magnetic saturation expands the high-efficiency range in the medium to high-speed rotation range from several thousand to 10,000 rpm. The insertion position of the magnetic composite material and the magnetic characteristics are also parameters of the variable magnetic flux. Both the insertion position and the magnetic properties of the magnetic composite material can be variables of the variable magnetic flux, resulting in improved variable magnetic flux controllability. Moreover, for high rotational speeds, mechanical stress tends to increase at the thin bridges between rotor magnets [43], [44]. Adjusting the insertion position of the composite magnetic material will also reduce mechanical stress.

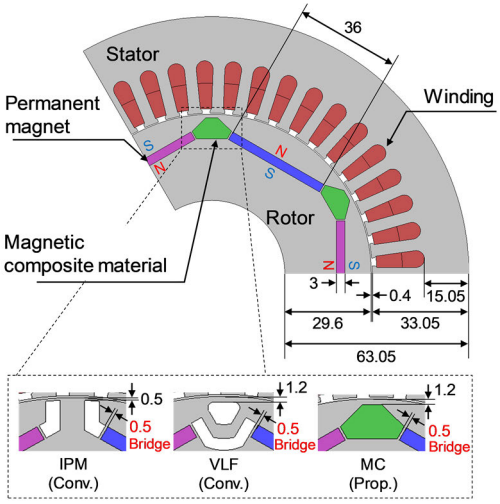


**FIGURE 1.** Structures of test motor (unit: mm).

Chapter 2 describes the characteristics of magnetic composite materials and the principle of MC motors. Chapter 3 explains the measurement results of the magnetic properties of the magnetic composite materials containing various magnetic powders. The simulation results indicate that variable magnetic flux is feasible. Furthermore, the obtained loss, when compared to conventional IPM and VLF motors, demonstrates the effect of the magnetic composite materials in enhancing maximum efficiency. The fourth chapter discusses the mechanical properties of the magnetic composite materials. A thicker bridge adjacent to the magnets may facilitate an increase in the high-efficiency area and a reduction in mechanical stress.

## II. VARIABLE MAGNETIC FLUX MOTOR USING MAGNETIC COMPOSITE MATERIAL

### A. MOTOR CONFIGURATION

Figure 1 depicts the configuration of the MC motor used in this paper. The MC motor is constructed by inserting a magnetic composite material into the flux barrier of the rotor.

For comparison, IPM and VLF motors are used; VLF motors have variable flux characteristics, similar to MC motors [33]. The test motor specifications are shown in Table 1; it has 6 poles and 45 slots, a stator with an outer diameter of 176.1 mm, and axial length of 100 mm. The stators of the three types of motors are the identical; the only difference is the configuration of the flux barrier between the rotor's permanent magnets.

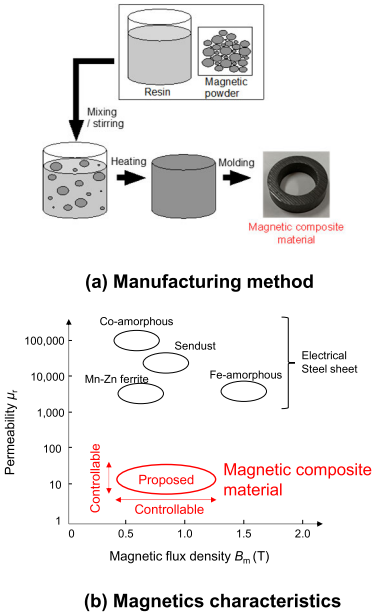


(a) Manufacturing method

(b) Magnetics characteristics

**FIGURE 2.** Characteristics of magnetic composite material.

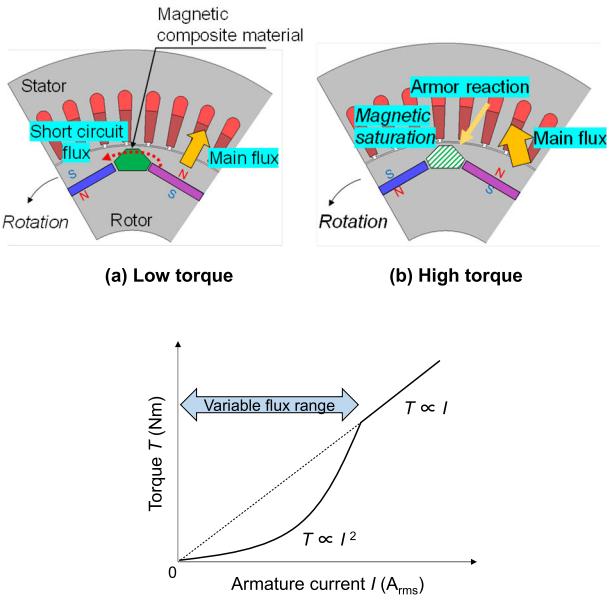


(a) Low torque

(b) High torque

(c) Torque characteristics

**FIGURE 3.** Principal of variable flux motor using magnetic composite material.

**TABLE 1.** Specification of test motor.

| Item | Value |
|---|---|
| Stator diameter | 176.1 mm |
| Rotor diameter | 110 mm |
| Axial length | 100 mm |
| Number of pole | 6 |
| Number of slots | 45 |
| Number of turns | 8×4 parallel |
| Diameter of coil | 2 mm |
| Magnet size | 36×3 mm |
| Stator core material | 35H300 (NIPPON STEEL CORPORATION) |
| Rotor core material | 35H300 (NIPPON STEEL CORPORATION) |
| Magnet type | N36Z (Shin-Etsu Chemical Co., Ltd.) |

### B. MAGNETIC COMPOSITE MATERIAL CHARACTERISTICS

The magnetic composite material is manufactured by mixing and sintering magnetic powder with resin as shown in Fig. 2(a). To prevent eddy currents and thus reduce iron loss in the magnetic composite material, the magnetic powder is dispersed and blended in the resin. This characteristic is effective in reducing iron loss in ultra-high-speed rotary motors of 100,000 rpm and high-frequency transformers of over 10 kHz [42], [45], [46]. Magnetic composite materials have lower magnetic permeability and saturation magnetic flux density than electrical steel sheets and other magnetic materials, as shown in Fig. 2(b). However, the saturation magnetic flux density and magnetic permeability can be easily adjusted by simply changing the material and compounding ratio of the magnetic composite material. Furthermore, no pressurizing process, such as a dust core, is required for manufacturing, allowing for the low-cost formation of a flexible structure (bulk or sheet) [38], [39], [40], [45].

### C. PRINCIPAL OF VARIABLE MAGNETIC FLUX

Figure 3 shows a cross-sectional configuration of an MC motor. The variable magnetic flux effect realized by utilizing the magnetic saturation of the magnetic composite material expands the high-efficiency range for the medium- to high-speed rotation range. The states of the magnetic flux under low torque and high torque action of the MC motor are shown in Figs. 3(a) and (b), respectively. At low torque, the magnet's flux is short-circuited via the composite material, reducing the number of magnetic fluxes linking the stator. The magnetic flux, however, is easily connected with the stator because the magnetic composite material is magnetically saturated as a result of the armature's reaction at high torque. The change in the magnetic flux through the stator results in the variable torque characteristics depicted in Fig. 3(c).

MC motors take benefit of the fact that magnetic composite materials are prone to magnetic saturation. Electrical steel sheets, which are frequently used in motor cores, have a saturation magnetic flux density of more than 1.5 T and a relative permeability of several thousand to 10,000 to avoid magnetic saturation and achieve high torque. The magnetic composite material, on the other hand, has a saturation magnetic flux density of approximately 1 T and a relative permeability of 10-50. Variable permeability has been demonstrated by inducing magnetic saturation of electrical steel sheets with additional stator windings [32]. The variable magnetic flux effect of the MC motor can be obtained without using additional windings by positively utilizing the magnetic saturation of the magnetic composite material.

**TABLE 2. Magnetic simulation conditions.**

| Item | Value |
|---|---|
| Software | JMAG-Designer (×64) Ver.20.2 |
| Analysis method | Two-dimensional magnetic field analysis |
| Mesh size | Copper :1/10 or less of the skin depth<br>Magnetic composite material: Automatic<br>Air : Automatic |
| Analysis area | Analysis in 3 times the analysis model |
| Material | Copper: $\rho = 1.72\times10^{-8}\Omega$m, $\mu_r' = 1$, $\mu_r'' = 0$<br>Magnetic composite material:<br>B-H curve and Iron loss profile in Fig. 5<br>Air : $\rho=\infty\ \Omega m$, $\mu_r' = 1$, $\mu_r'' = 0$ |
| Control | MTPA (Maximum torque per ampere) and weakening field control |
| Efficiency map | Stator: copper loss of coil and iron loss of core<br>Rotor: iron loss of core, permanent magnet, and magnetic composite material |
| DC voltage | 280 V |
| PWM frequency | 20 kHz |

**TABLE 3. Comparison of high efficiency area.**

| Motor | 96% area | 94% area |
|---|---|---|
| IPM | × 1.0 (Ref.) | × 1.0 (Ref.) |
| VLF | × 2.1 | × 1.2 |
| MC | × 2.5 | × 1.4 |
| (MC with Fe-AMO) | × 2.1 | × 1.2 |
| (MC with Fe-Si) | × 2.2 | × 1.2 |

### D. MC MOTOR ADVANTAGES

The following advantages are expected for MC motors by using magnetic composite materials.

1) The variable magnetic flux effect, which takes advantage of the magnetic saturation of the magnetic composite material, suppresses the weakening field current during medium- to high-speed rotation, lowering copper loss. Compared to the VLF motor, inserting a magnetic composite between the permanent magnets results in a higher q-axis inductance, which increases the reluctance torque in the field-weakening region.

2) The use of a magnetic composite material between permanent magnets reduces the variation of rotor reluctance with rotation angle, thereby suppressing spatial harmonics. This effect reduces iron loss in the medium to high speed range.

The effects of 1) and 2) expand the high efficiency range in the medium to high-speed range as shown in Fig. 4.

3) The magnetic characteristics, as well as the position of the magnetic composite material, influence the variable magnetic flux characteristics of the MC motor. Increased the variable flux parameter improves mechanical strength, resulting in flexible motor design.

## III. MOTOR EFFICIENCY CHARACTERISTICS

### A. MAGNETIC PROPERTIES OF MAGNETIC COMPOSITE MATERIALS

Figures 5(a) and 5(b) reveal the measurement results of the iron loss characteristics and magnetization characteristics,

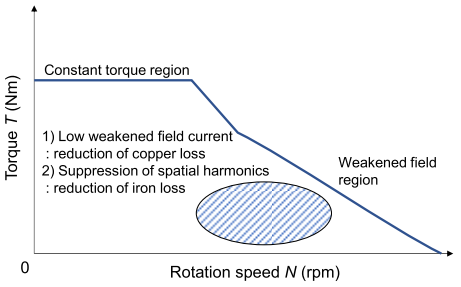


**FIGURE 4. Effects on high efficiency of MC motor.**

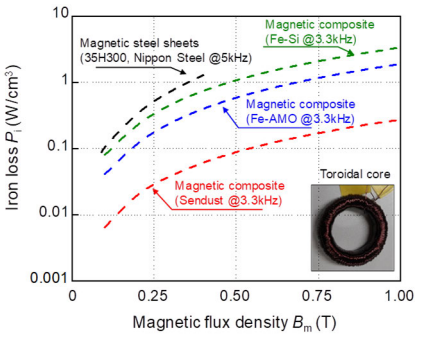


**(a) Iron loss characteristics**

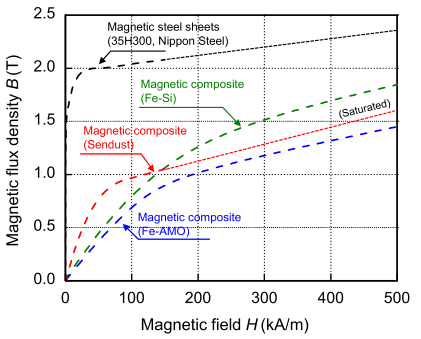


**(b) Magnetization curve**

**FIGURE 5. Magnetic properties of magnetic composite material.**

respectively. The iron loss characteristics were measured with a B-H analyzer (SY-8218: IWATSU ELECTRIC CO., LTD.).

The magnetic composite material uses Fe–Si–Al (Sendust) magnetic powder with an average particle size of 40 $\mu$m and epoxy resin. The magnetic composite material was created by mixing, stirring, and firing magnetic powder at a volume ratio of 69 vol.%. The magnetic powders of the magnetic composite materials were prepared using Fe-amorphous alloy of 64 vol.% (Fe-AMO) and Fe-silicon of 67 vol.% (Fe-Si). The mixing ratio for each magnetic powder is the upper limit value considering the viscosity of the material.

When compared to other materials, the iron loss of the magnetic composite material using Sendust is the lowest. Magnetic composite materials have lower saturation magnetic flux density and relative magnetic permeability than

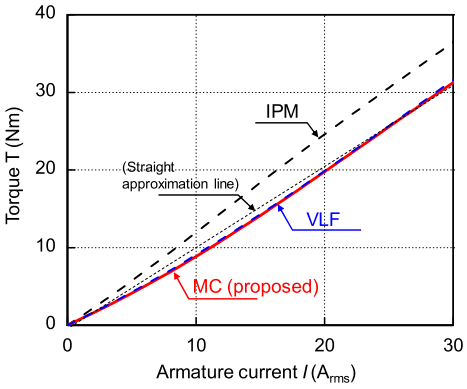


**FIGURE 6.** Torque characteristics.

magnetic steel sheets. Sendust magnetization properties are intermediate between the other two types. The complex specific magnetic flux real part $\mu_r$' is 16, and the saturation magnetic flux density $B_s$ is 0.8 T. The magnetic composite material with Sendust, which has the lowest core loss, is used for the MC motor.

### B. TORQUE CHARACTERISTICS

Electromagnetic field simulation shows the torque characteristics, efficiency characteristics and loss characteristics of MC motors. The analysis conditions are shown in Table 2; and the two-dimensional finite element method of JMAG-Designer is employed. In the analysis, the magnetic properties of magnetic saturation are approximated by extrapolation. Figure 6 illustrates the torque characteristics of the MC and IPM motors. The torque constant of the IPM motor is larger than the MC motor and has linearity with respect to the current. The MC motor, on the other hand, has a larger curvature at low current than the linear approximation line and returns to linear at high torque, indicating the effect of the variable magnetic flux motor [33]. At low torque/high-speed rotation, this effect reduces the counter electromotive force constant, suppressing the field weakening current and lowering copper loss.

Figure 7 depicts the magnetic flux density distribution of the MC motor. At zero load, the permanent magnet's magnetic flux short-circuits the rotor, while the stator's interlinkage magnetic flux is suppressed. A high current expands the saturation region of the magnetic composite material. At a 30-A load, most of the magnetic composites are magnetically saturated above 1 T, and the flux interlinking of the stator is increasing. The magnetic flux distribution in the MC motor changes with the current, indicating that the magnetic composite material realizes variable magnetic flux. The MC motor uses the same principle as the VLF motor to achieve variable magnetic flux, which can change the amount of leakage magnetic flux.

### C. EFFICIENCY CHARACTERISTICS

Figure 8 shows the efficiency characteristics of IPM, VLF and MC motors. The maximum efficiency range of MC motors has been increased to over 5,000 rpm. In addition, the range of efficiency of 94% has been expanded to over 8,000 rpm, and the efficiency at high-speed rotation of 15,000 rpm has also improved to 90% in MC motor. Compared to the 96% area of IPM motor, the maximum torque of MC motor is almost the same, and the maximum speed is increased by more than 2,000 rpm. Similarly, the maximum speed of MC motor is approximately 500 rpm higher than that of VLF motor. Table 3 shows the comparison of the high-efficiency areas. VLF and MC motors have a maximum efficiency area exceeding 96%, more than twice that of IPM motors. In the 96% efficiency region, the MC motor has a lower maximum torque but a higher maximum speed. The efficiency expansion effect of MC motors using Fe-AMO and Fe–Si is almost the same as that of VLF motors, but they are smaller than MC motors using Sendust.

### D. LOSS CHARACTERISTICS

The copper loss and field weaken current (d-axis current) maps will be used to confirm the factors for expanding the high-efficiency range. Figure 9 is a copper loss map of each motor, which shows that the copper loss of MC motors in the high-speed rotation range at 10,000 rpm is reduced by about 50% compared to IPM motor. The copper loss of MC motors in the high speed range is smaller than that of IPM and VLF motors. Figure 10 depicts the d-axis current of each motor. At 10,000 rpm, the MC motor can reduce the d-axis current by about 25 A and 10 A compared to IPM and VLF motors, respectively, which is the primary factor in reducing copper loss. The variable magnetic flux with the magnetic composite material can improves motor efficiency.

Figure 11 is an iron loss map of each motor. The iron loss in the high-speed rotation region of the MC motor around 10,000 rpm is reduced by nearly 70% and 10% compared to IPM and VLF motors, respectively, which is a factor for improving efficiency in the same way as the copper loss. Figure 12 shows the result of Fourier transforming the magnetic flux density in the gap between the stator and the rotor. Spatial harmonics above 2 kHz are greatly reduced in MC motors, which contributes to lower iron loss.

Table 4 shows the comparison of the loss of MTPA (Maximum torque per ampere) control, 8,000 rpm and 10 Nm drive, in weakened field domain. Because of the low phase current operation, the MC motor has a 32.7% lower current than the IPM motor, which greatly reduces copper loss. Space harmonic suppression is effective in lowering stator and rotor iron losses. The magnetic composite material has almost no iron loss, which contributes to a reduction in rotor iron loss.

The copper and iron losses of the MC motor are reduced by 28% and 27%, respectively, when compared to the VLF motor. Copper loss is reduced not only by lowering field-weakening currents based on variable field magnetism but also by increasing saliency. As shown Table 4, the MC motor has a higher saliency ratio than the VLF motor, resulting in higher reluctance torque. VLF and MC motors,

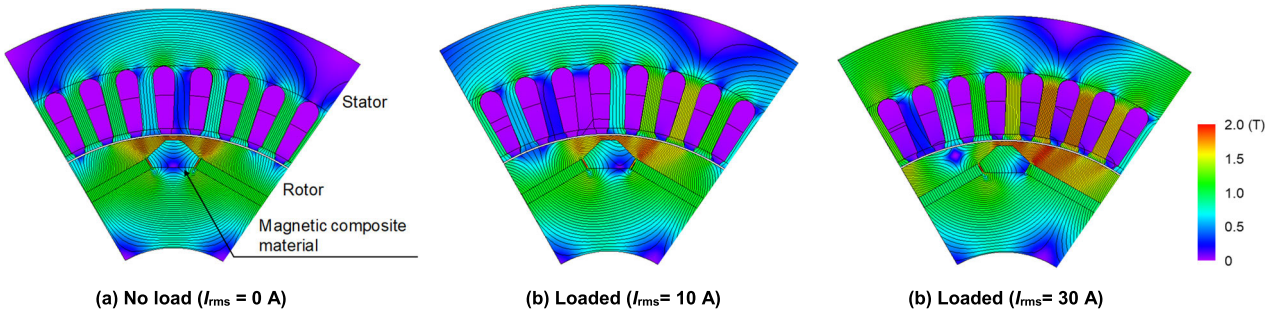


**FIGURE 7.** Magnetic flux distributions of MC motor.

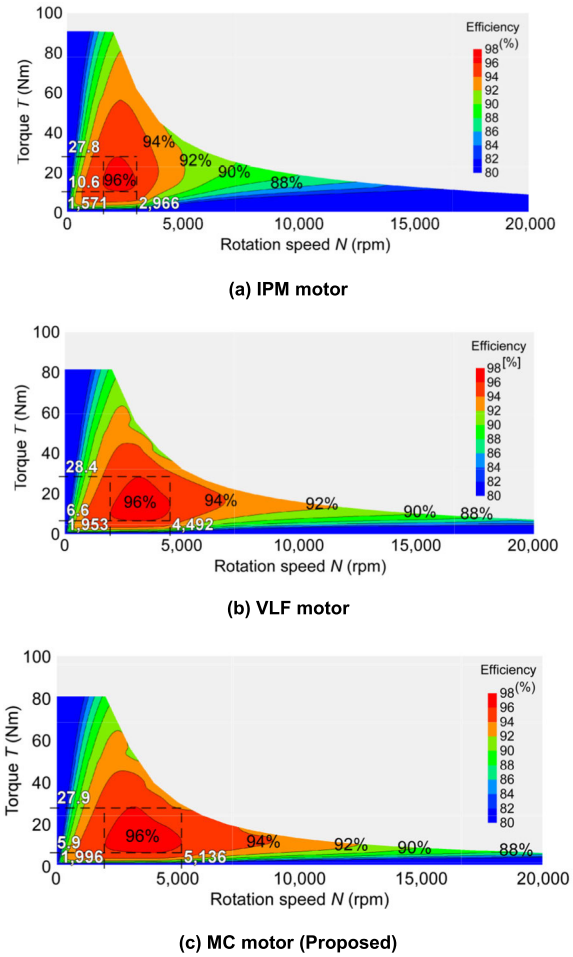


**FIGURE 8.** Efficiency map.

however, have significantly lower q-axis inductance than IPM motors, which contributes to lower maximum torque.

The suppression of spatial harmonics and the reduction of stator flux linkage affect the reduction of iron loss in MC motors. The result of Fourier transforming the magnetic flux density in the gap between the stator and rotor is shown in Figure 12. In MC motors configurable without flux barriers, spatial harmonics above 2 kHz are greatly reduced, contributing to lower rotor iron loss. The maximum interlinkage magnetic flux of the stator for the VLF and MC motors is 1.83T and 1.75T, respectively, with the difference also being one of the factors reducing the MC motor's stator iron loss.

**TABLE 4.** Comparison of losses.

| Item | IPM | VLF | MC |
|---|---|---|---|
| Rotation condition | 8,000 rpm·10 Nm | | |
| Current $I$ ($A_{rms}$) | 43.4 | 34.5 | 29.2 |
| Current phase $\theta_e$ (deg) | 84.4 | 77.4 | 76.2 |
| Inductance of d-axis $L_d$ (mH) | 2.1 | 1.9 | 2.0 |
| Inductance of q-axis $L_q$ (mH) | 5.3 | 3.5 | 4.5 |
| Saliency | 2.5 | 1.8 | 2.3 |
| Copper loss $P_c$ (W) | 642.7 | 406.6 | 291.0 |
| Iron loss in stator $P_{is}$ (W) | 643.1 | 239.4 | 170.9 |
| Iron loss in rotor $P_{ir}$ (W) | 107.5 | 54.0 | 41.3 |
| Iron loss in magnet $P_{im}$ (W) | 37.5 | 1.2 | 1.8 |
| Iron loss in magnetic composite material $P_{ic}$ (W) | - | - | 0.1 |
| Efficiency $\eta$ (%) | 85.4 | 92.3 | 94.3 |

## IV. RELIEF OF MECHANICAL STRESS

In Section III, the effect of widening the high efficiency range with variable magnetic flux was confirmed by using a magnetic composite material composed of Sendust. This section explains how the size of the magnetic composite affects the motor's high-efficiency area and mechanical stress.

### A. MECHANICAL PROPERTIES OF MAGNETIC COMPOSITE MATERIALS

A dumbbell-shaped specimen was used to test the tensile strength of the magnetic composite material with Sendust. To measure the elongation, a strain gauge (KFG-10-120-C1-1L1M2R; Kyowa Dengyo Co., Ltd.) was attached to the center of the measurement sample. A tensile tester was used to measure the tensile load and strain gauge displacement at 1 mm/min (Autograph AG-300kN Xplus; Shimadzu Corporation).

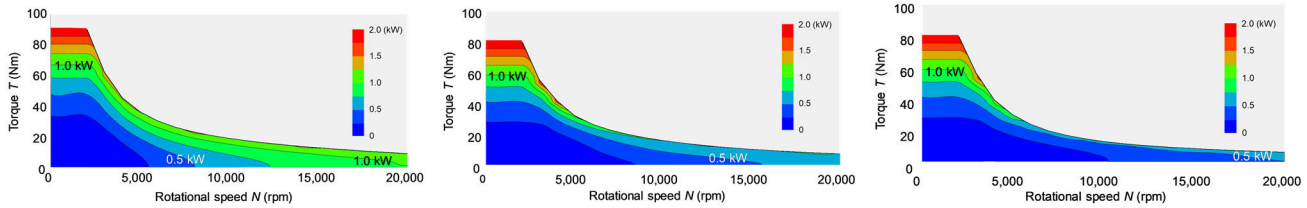


(a) IPM motor (b) VLF motor (c) MC motor (proposed)

**FIGURE 9.** Copper loss map.

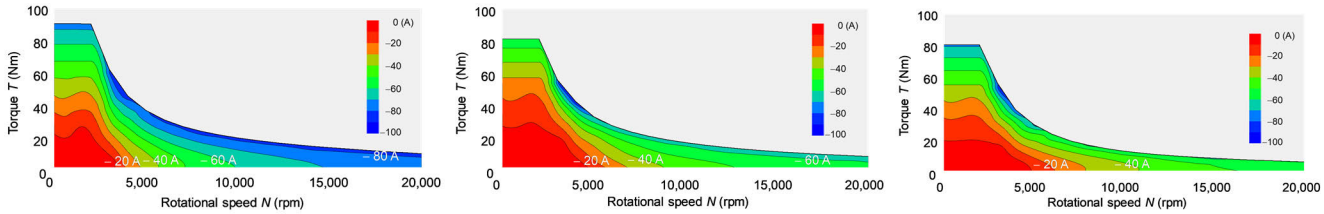


(a) IPM motor (b) VLF motor (c) MC motor (proposed)

**FIGURE 10.** Field weakened current map.

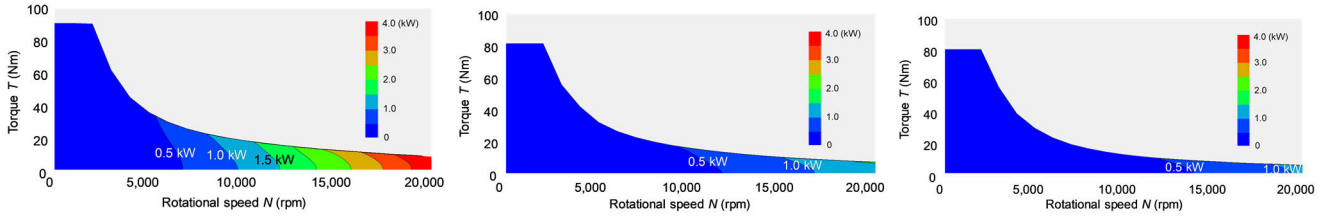


(a) IPM motor (b) VLF motor (c) MC motor (proposed)

**FIGURE 11.** Iron loss map.

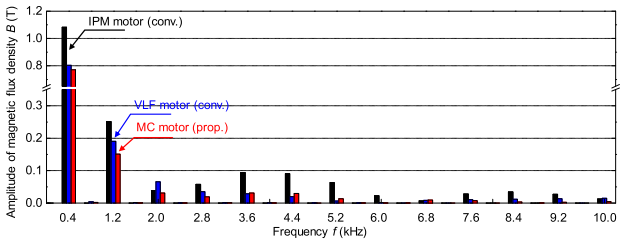


**FIGURE 12.** Spectrum of magnetic flux density ($N = 8000$ rpm).

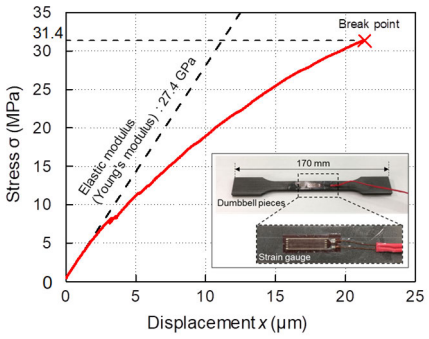


**FIGURE 13.** Stress in magnetic composite materials.

The results of stress measurements are shown in Figure 13, which show that the magnetic composite barely stretches to its maximum breaking strength. The tensile and breaking strengths are both 31.4 MPa, and the longitudinal modulus of elasticity (Young's modulus) is 27.4 GPa. The ultrasonic method yielded a poisson's ratio of 0.28. According to the water displacement method, the weight density is 5.32 kg/m$^3$.

### B. VON MISES STRESS COMPARISON

The von Mises stress is often used for strength analysis of the bridge part of electrical steel sheets [33], [47]. This paper also focuses on the stress analysis of the bridge part

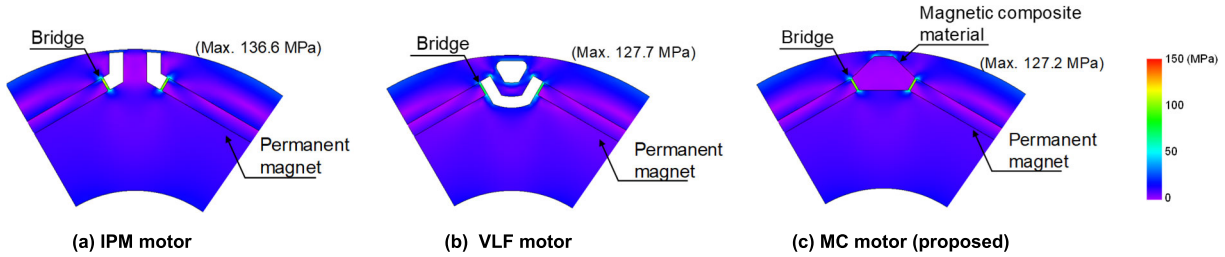


**FIGURE 14.** Mises stress distribution ($N$ = 8000 rpm).

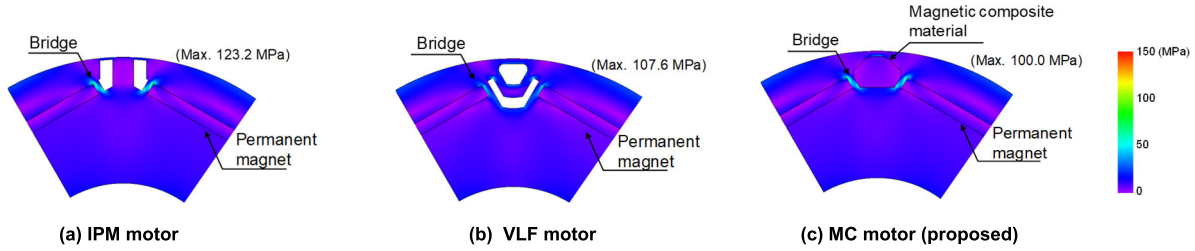


**FIGURE 15.** Mises stress distribution with stress reduction model ($N$ = 8000 rpm).

**TABLE 5.** Structural simulation conditions.

| Item | Value |
|---|---|
| Software | JMAG-Designer (×64) Ver.20.2 |
| Analysis method | Two-dimensional structural analysis |
| Rotation speed | 8000 rpm |
| Mesh size | Magnetic composite material : 0.2 mm<br>Rotor core and permanent magnet: 0.4 mm |
| Material | Rotor core: 35H300<br>$E$=21.0 GPa, $\nu$= 0.30, $\rho$ = 7.65 kg/m$^3$<br>Permanent magnet: N36Z<br>$E$=15.0 GPa, $\nu$= 0.23, $\rho$ = 7.70 kg/m$^3$<br>Magnetic composite material: Sendust 69vol.%<br>$E$=27.4 GPa, $\nu$= 0.28, $\rho$ = 5.32 kg/m$^3$ |
| Contact | All sides (permanent magnets, magnetic composite materials) finite slip |
| Adhesion | All sides (permanent magnets, magnetic composite materials) layer 0.1mm, $E$=0.025 MPa |

of electrical steel sheets. The von Mises stress of the motor rotor at 8,000 rpm was evaluated by the two-dimensional finite element method structural analysis of JMAG-Designer. Table 5 shows the conditions for structural analysis, where the physical properties of the magnetic composite material are the measurement results. Contact and adhesion conditions were considered for the permanent magnets and magnetic composites. The maximum tensile stress of magnetic composites assumed to be brittle materials was also analyzed.

Figure 14 shows the results of von Mises stress analysis. The von Mises stress of the magnetic composite material is significantly less than its tensile strength, thus providing adequate resistance to centrifugal force. The stress at the bridge between the magnet and air gap tend to be high. IPM, VLF and MC motors have maximum stress values of 136.6, 127.7, and 127.2 MPa, respectively. The maximum tensile stress of the magnetic composite is 3.34 MPa, which is smaller than the break point as shown Fig. 13.

### C. RELATIONSHIP BETWEEN BRIDGE THICKNESS AND HIGH-EFFICIENCY AREA

Increasing the width of the bridge is effective in relieving stress. Meanwhile, larger bridge's width increases magnetic flux short-circuiting and tends to diminish motor torque. The analysis confirmed the effect of increasing the bridge spacing on von Mises stress and the maximum efficiency region.

The spacing between the bridges in Fig. 1 has been increased from 0.5 to 1.5 mm. Figure 15 depicts each motor's von Mises stress distribution. IPM, VLF and MC motors have respective maximum stress values of 123.2, 107.6, and 100.0 MPa. The bridge portion of the motor rotor can be substantially de-stressed. The maximum tensile stress of the magnetic composite of the motor with widened bridge is 4.46 MPa, which is also smaller than the break point as shown Fig. 13.

Figure 16 depicts the efficiency maps of IPM, VLF, and MC motors with respect to the stress relaxation type. The numbers in parentheses represent the 96% region values of the motors without enlarging the bridge in Fig. 8. The 96% area of all stress relaxation-type motors extends to the high-speed section. While the maximum torque value in the 96% region decreased significantly for the stress relaxation type IPM and VLF motors, the rate of decrease was small for the MC motor. By adjusting the size of the magnetic composite material, both stress relief and expansion of the high-efficiency region are accomplished.

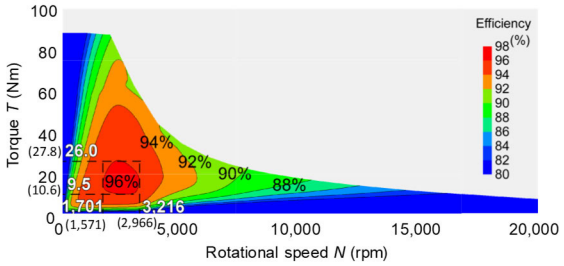


(a) IPM motor

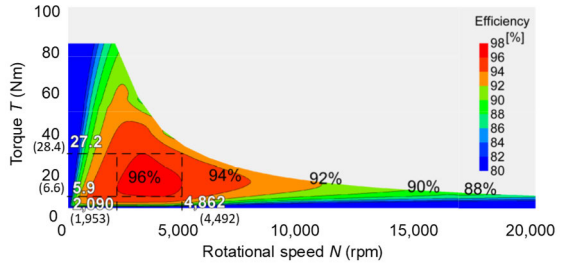


(b) VLF motor

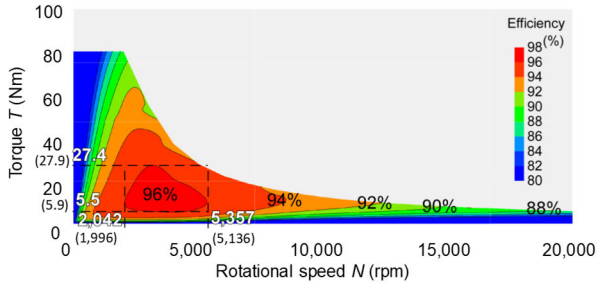


(c) MC motor (Proposed)

**FIGURE 16.** Efficiency map (Stress reduction model).

## V. CONCLUSION

This study proposes a variable magnetic flux motor that utilizes magnetic saturation by embedding a magnetic composite material in a rotor. Magnetic composite materials exhibit significantly lower saturation magnetic flux density and magnetic permeability than electrical steel sheets. Their magnetic properties are controlled by changing the mixing ratio of the magnetic powder of the material. The proposed technique achieves a torque curve at a low load, implying that variable magnetic flux is generated by using a magnetic composite material. The proposed motor reduced current by 32.7% at 8,000 rpm due to its lower phase. Furthermore, the MC motor suppressed spatial harmonics and reduced iron loss 72.8% compared with IPM motor. Because of these loss reduction effects, the high efficiency range of 96% was expanded to more than twice that of the IPM motor. Furthermore, the mechanical stress is affected by the thickness of the bridge between rotor's permanent magnets. Based on magnetic composite material's physical property measurement results, the effect of bridge distance on the high-efficiency area and mechanical stress relaxation was confirmed. The MC motor with a broader bridge has lesser torque loss than other motors and can reduce the most stress.

## REFERENCES

[1] W. Jiang, S. Feng, Z. Zhang, J. Zhang, and Z. Zhang, "Study of efficiency characteristics of interior permanent magnet synchronous motors," *IEEE Trans. Magn.*, vol. 54, no. 11, pp. 1–5, Nov. 2018, doi: 10.1109/TMAG.2018.2847328.

[2] H.-C. Chuang, G.-D. Li, and C.-T. Lee, "The efficiency improvement of AC induction motor with constant frequency technology," *Energy*, vol. 174, pp. 805–813, May 2019, doi: 10.1016/j.energy.2019.03.019.

[3] S.-K. Cho, K.-H. Jung, and J.-Y. Choi, "Design optimization of interior permanent magnet synchronous motor for electric compressors of air-conditioning systems mounted on EVs and HEVs," *IEEE Trans. Magn.*, vol. 54, no. 11, pp. 1–5, Nov. 2018, doi: 10.1109/TMAG.2018.2849078.

[4] A. Balamurali, G. Feng, C. Lai, J. Tjong, and N. C. Kar, "Maximum efficiency control of PMSM drives considering system losses using gradient descent algorithm based on DC power measurement," *IEEE Trans. Energy Convers.*, vol. 33, no. 4, pp. 2240–2249, Dec. 2018, doi: 10.1109/TEC.2018.2852219.

[5] S. Li, C. Gu, P. Zhao, and S. Cheng, "A novel hybrid propulsion system configuration and power distribution strategy for light electric aircraft," *Energy Convers. Manag.*, vol. 238, Jun. 2021, Art. no. 114171, doi: 10.1016/j.enconman.2021.114171.

[6] H.-J. Park and M.-S. Lim, "Design of high power density and high efficiency wound-field synchronous motor for electric vehicle traction," *IEEE Access*, vol. 7, pp. 46677–46685, 2019, doi: 10.1109/ACCESS.2019.2907800.

[7] Y. Yang, Q. He, C. Fu, S. Liao, and P. Tan, "Efficiency improvement of permanent magnet synchronous motor for electric vehicles," *Energy*, vol. 213, Dec. 2020, Art. no. 118859, doi: 10.1016/j.energy.2020.118859.

[8] Y. Feng, F. Li, S. Huang, and N. Yang, "Variable-flux outer-rotor permanent magnet synchronous motor for in-wheel direct-drive applications," *Chin. J. Elect. Eng.*, vol. 4, no. 1, pp. 28–35, Mar. 2018, doi: 10.23919/CJEE.2018.8327368.

[9] X. Hu, H. Chen, Z. Li, and P. Wang, "An energy-saving torque vectoring control strategy for electric vehicles considering handling stability under extreme conditions," *IEEE Trans. Veh. Technol.*, vol. 69, no. 10, pp. 10787–10796, Oct. 2020, doi: 10.1109/TVT.2020.3011921.

[10] G. Hong, T. Wei, and X. Ding, "Multi-objective optimal design of permanent magnet synchronous motor for high efficiency and high dynamic performance," *IEEE Access*, vol. 6, pp. 23568–23581, 2018, doi: 10.1109/ACCESS.2018.2828802.

[11] M. Malekpour, R. Azizipanah-Abarghooee, and V. Terzija, "Maximum torque per ampere control with direct voltage control for IPMSM drive systems," *Int. J. Electr. Power Energy Syst.*, vol. 116, Mar. 2020, Art. no. 105509, doi: 10.1016/j.ijepes.2019.105509.

[12] Q. Li, T. Fan, and X. Wen, "Characterization of iron loss for integral-slot interior permanent magnet synchronous machine during flux weakening," *IEEE Trans. Magn.*, vol. 53, no. 5, pp. 1–8, May 2017, doi: 10.1109/TMAG.2017.2676094.

[13] J. Liu, C. Gong, Z. Han, and H. Yu, "IPMSM model predictive control in flux-weakening operation using an improved algorithm," *IEEE Trans. Ind. Electron.*, vol. 65, no. 12, pp. 9378–9387, Dec. 2018, doi: 10.1109/TIE.2018.2818640.

[14] H. Wei, J. Yu, Y. Zhang, and Q. Ai, "High-speed control strategy for permanent magnet synchronous machines in electric vehicles drives: Analysis of dynamic torque response and instantaneous current compensation," *Energy Rep.*, vol. 6, pp. 2324–2335, Nov. 2020, doi: 10.1016/j.egyr.2020.08.016.

[15] W. Xu, M. M. Ismail, Y. Liu, and M. R. Islam, "Parameter optimization of adaptive flux-weakening strategy for permanent-magnet synchronous motor drives based on particle swarm algorithm," *IEEE Trans. Power Electron.*, vol. 34, no. 12, pp. 12128–12140, Dec. 2019, doi: 10.1109/TPEL.2019.2908380.

[16] N. Matsui, "Design and control of variable field permanent magnet motors," *IEEJ Trans. Electr. Electron. Eng.*, vol. 14, no. 7, pp. 966–981, Jul. 2019, doi: 10.1002/tee.22891.

[17] R. Jayarajan, N. Fernando, and I. U. Nutkani, "A review on variable flux machine technology: Topologies, control strategies and magnetic materials," *IEEE Access*, vol. 7, pp. 70141–70156, 2019, doi: 10.1109/ACCESS.2019.2918953.

[18] M. Aoyama and T. Noguchi, "Study and experimental performance evaluation of flux intensifying PM motor with variable leakage magnetic flux," *Electr. Eng. Jpn.*, vol. 207, no. 4, pp. 36–54, Jun. 2019, doi: 10.1002/eej.23162.

[19] V. Ostovic, "Pole-changing permanent-magnet machines," *IEEE Trans. Ind. Appl.*, vol. 38, no. 6, pp. 1493–1499, Nov. 2002, doi: 10.1109/TIA.2002.805568.

[20] R. Owen, Z. Q. Zhu, J. B. Wang, D. A. Stone, and I. Urquhart, "Review of variable-flux permanent magnet machines," in *Proc. Int. Conf. Electr. Mach. Syst.*, Aug. 2011, pp. 1–6, doi: 10.1109/ICEMS.2011.6073754.

[21] Z. Zhou, H. Hua, and Z. Zhu, "Flux-adjustable permanent magnet machines in traction applications," *World Electric Vehicle J.*, vol. 13, no. 4, p. 60, Mar. 2022, doi: 10.3390/wevj13040060.

[22] K. Sakai, K. Yuki, Y. Hashiba, N. Takahashi, K. Yasui, and L. Kovudhikulrungsri, "Principle and basic characteristics of variable-magnetic-force memory motors," *IEEJ Trans. Ind. Appl.*, vol. 131, no. 1, pp. 53–60, 2011, doi: 10.1541/ieejias.131.53.

[23] T. Kato, N. Limsuwan, C.-Y. Yu, K. Akatsu, and R. D. Lorenz, "Rare earth reduction using a novel variable magnetomotive force flux-intensified IPM machine," *IEEE Trans. Ind. Appl.*, vol. 50, no. 3, pp. 1748–1756, May/Jun. 2014, doi: 10.1109/TIA.2013.2283314.

[24] H. Liu, H. Lin, Z. Q. Zhu, M. Huang, and P. Jin, "Permanent magnet remagnetizing physics of a variable flux memory motor," *IEEE Trans. Magn.*, vol. 46, no. 6, pp. 1679–1682, Jun. 2010, doi: 10.1109/TMAG.2010.2044638.

[25] K. Sakai and K. Matsuda, "Permanent magnet motor with reversible salient poles and variable magnetic force," *IEEJ J. Ind. Appl.*, vol. 6, no. 1, pp. 19–28, 2017, doi: 10.1541/ieejjia.6.19.

[26] Z. Q. Zhu and D. Howe, "Electrical machines and drives for electric, hybrid, and fuel cell vehicles," *Proc. IEEE*, vol. 95, no. 4, pp. 746–765, Apr. 2007, doi: 10.1109/JPROC.2006.892482.

[27] Y. Xie, Z. Ning, and Z. Ma, "Comparative study on variable flux memory machines with different arrangements of permanent magnets," *IEEE Access*, vol. 8, pp. 164304–164312, 2020, doi: 10.1109/ACCESS.2020.3022595.

[28] L. Chen, D. Hopkinson, J. Wang, A. Cockburn, M. Sparkes, and W. O'Neill, "Reduced dysprosium permanent magnets and their applications in electric vehicle traction motors," *IEEE Trans. Magn.*, vol. 51, no. 11, pp. 1–4, Nov. 2015, doi: 10.1109/TMAG.2015.2437373.

[29] J. M. D. Coey, "New permanent magnets; Manganese compounds," *J. Phys., Condens. Matter*, vol. 26, no. 6, Feb. 2014, Art. no. 064211, doi: 10.1088/0953-8984/26/6/064211.

[30] K. Sone, M. Takemoto, S. Ogasawara, K. Takezaki, and H. Akiyama, "A ferrite PM in-wheel motor without rare earth materials for electric city commuters," *IEEE Trans. Magn.*, vol. 48, no. 11, pp. 2961–2964, Nov. 2012, doi: 10.1109/TMAG.2012.2196685.

[31] T. Nonaka, S. Oga, and M. Ohto, "Consideration about the drive of variable magnetic flux motor," *IEEJ Trans. Ind. Appl.*, vol. 135, no. 5, pp. 451–456, 2015, doi: 10.1541/ieejias.135.451.

[32] K. Iwama and T. Noguchi, "Operation characteristics of adjustable field IPMSM utilizing magnetic saturation," *Energies*, vol. 15, no. 1, p. 52, Dec. 2021, doi: 10.3390/en15010052.

[33] T. Kato, M. Minowa, H. Hijikata, K. Akatsu, and R. D. Lorenz, "Design methodology for variable leakage flux IPM for automobile traction drives," *IEEE Trans. Ind. Appl.*, vol. 51, no. 5, pp. 3811–3821, Sep./Oct. 2015, doi: 10.1109/TIA.2015.2439642.

[34] X. Cai, Q. Wang, Y. Wang, and L. Zhang, "Research on a variable-leakage-flux permanent magnet motor control system based on an adaptive tracking estimator," *Energies*, vol. 16, no. 2, p. 587, Jan. 2023, doi: 10.3390/en16020587.

[35] J. Hang, S. Ding, X. Ren, Q. Hu, Y. Huang, W. Hua, and Q. Wang, "Integration of interturn fault diagnosis and torque ripple minimization control for direct-torque-controlled SPMSM drive system," *IEEE Trans. Power Electron.*, vol. 36, no. 10, pp. 11124–11134, Oct. 2021, doi: 10.1109/TPEL.2021.3073774.

[36] M. Horiuchi, R. Masuda, Y. Bu, M. Nirei, M. Sato, and T. Mizuno, "Effect of magnetic wedge characteristics on torque ripple and loss in interior permanent magnet synchronous motor," *IEEJ J. Ind. Appl.*, vol. 11, no. 1, pp. 49–58, Jan. 2022, doi: 10.1541/ieejjia.21002574.

[37] N. Yabu, K. Sugimura, M. Sonehara, and T. Sato, "Fabrication and evaluation of composite magnetic core using iron-based amorphous alloy powder with different particle size distributions," *IEEE Trans. Mag.*, vol. 54, no. 11, pp. 1–5, Nov. 2018, doi: 10.1109/TMAG.2018.2832662.

[38] M. Sato, K. Sugimoto, K. Kubota, S. Endo, and T. Mizuno, "Reducing the alternating current resistance and heat generation in a single-wire coil using a magnetic tape," *IEEJ Trans. Electr. Electron. Eng.*, vol. 15, no. 10, pp. 1541–1548, Oct. 2020, doi: 10.1002/tee.23224.

[39] M. Sato, Y. Hattori, M. Ueda, Y. Bu, and T. Mizuno, "Improved performance of a flat-wire coil with magnetic composite material for wireless power transfer," *IEEE Mag. Lett.*, vol. 12, pp. 1–5, 2021, doi: 10.1109/LMAG.2021.3075937.

[40] M. Sato, M. Nirei, Y. Yamanaka, T. Suzuki, Y. Bu, and T. Mizuno, "Increasing the efficiency of a drone motor by arranging magnetic sheets to windings," *Energy Rep.*, vol. 6, pp. 439–446, Feb. 2020, doi: 10.1016/j.egyr.2019.11.100.

[41] M. Sato, K. Takazawa, M. Horiuchi, R. Masuda, R. Yoshida, M. Nirei, Y. Bu, and T. Mizuno, "Reducing rotor temperature rise in concentrated winding motor by using magnetic powder mixed resin ring," *Energies*, vol. 13, no. 24, p. 6721, Dec. 2020, doi: 10.3390/en13246721.

[42] R. Yoshida, M. Tanaka, R. Masuda, M. Horiuchi, K. Takazawa, M. Sato, T. Mizuno, and M. Nirei, "Reduction of iron loss in ultrahigh-speed interior winding synchronous motor using magnetic composite material," in *Proc. 24th Int. Conf. Electr. Mach. Syst. (ICEMS)*, Oct. 2021, pp. 387–392, doi: 10.23919/ICEMS52562.2021.9634410.

[43] J. -W. Jung, B. -H. Lee, D. -J. Kim, J. -P. Hong, J. -Y. Kim, S. -M. Jeon, and D. -H. Song, "Mechanical stress reduction of rotor core of interior permanent magnet synchronous motor," *IEEE Trans. Magn.*, vol. 48, no. 2, pp. 911–914, Feb. 2012, doi: 10.1109/TMAG.2011.2172582.

[44] J.-H. Kim, D.-M. Kim, Y.-H. Jung, and M.-S. Lim, "Design of ultra-high-speed motor for FCEV air compressor considering mechanical properties of rotor materials," *IEEE Trans. Energy Convers.*, vol. 36, no. 4, pp. 2850–2860, Dec. 2021, doi: 10.1109/TEC.2021.3062646.

[45] K. Shimura, K. Kubota, M. Sato, T. Mizuno, M. Sakurada, T. Nebashi, and N. Koike, "Alternating-current copper loss reduction in a high-frequency transformer for railways using a magnetic tape," *IEEE Trans. Magn.*, vol. 57, no. 11, pp. 1–7, Nov. 2021, doi: 10.1109/TMAG.2021.3113498.

[46] T. Suzuki, M. Nirei, T. Yamamoto, Y. Yamanaka, T. Goto, M. Sato, Y. Bu, and T. Mizuno, "Reduction of eddy currents in winding by using a magnetic layer on an IPM motor," *IEEJ Trans. Electr. Electron. Eng.*, vol. 15, no. 4, pp. 601–606, Apr. 2020, doi: 10.1002/tee.23094.

[47] K. Yamazaki and Y. Kato, "Optimization of high-speed motors considering centrifugal force and core loss using combination of stress and electromagnetic field analyses," *IEEE Trans. Magn.*, vol. 49, no. 5, pp. 2181–2184, May 2013, doi: 10.1109/TMAG.2013.2244587.

**MITSUHIDE SATO** (Member, IEEE) was born in May 1986. He received the B.E. and M.E. degrees from Tohoku University, Sendai, Japan, in 2009 and 2011, respectively, and the Ph.D. degree from Shinshu University, Nagano, Japan, in 2019.

From 2011 to 2015, he was an Electrical Engineer with Toshiba Corporation, Japan. From 2015 to 2019, he was a Lecturer with the Nagano Prefectural Institute of Technology, Ueda, Japan. He is currently an Assistant Professor with the Department of Engineering, Shinshu University. His research interests include electrical equipment and power electronics. He is a Senior Member of the Institute of Electrical Engineers of Japan (IEEJ) and a member of the Japan Society of Applied Electromagnetics and Mechanics (JSAEM).

**KEIGO TAKAZAWA** is currently a Technical Staff with the Department of Engineering, Shinshu University, Japan.

**RYO YOSHIDA** received the B.E. degree from Shinshu University, Nagano, Japan, in 2021, where he is currently pursuing the M.E. degree. His research interest includes permanent magnet synchronous motor.

**MASAMI NIREI** (Member, IEEE) received the B.E., M.E., and D.E. degrees in electrical engineering from Shinshu University. He was an Engineer with Gunma NEC, from 1988 to 1990. In 1990, he joined the Shinshu University Hospital as an Assistant Professor, and he was transferred to the National Institute of Technology, Nagano College, in 1991, where he is currently a Professor with the Department of Electronics and Computer Science. His research interests include electromagnetic actuators and sensors, optimal design, and numerical analysis. He is a member of the Magnetics Society of Japan and the Japan Society of Applied Electromagnetics and Mechanics.

**TSUTOMU MIZUNO** (Senior Member, IEEE) was born in June 1958. He received the B.E., M.E., and Ph.D. degrees in engineering from Shinshu University, Nagano, Japan, in 1981, 1983, and 1994, respectively. From 1983 to 1996, he was an Electrical Engineer with Amada Company Ltd., Japan. From 1996 to 1999, he was an Assistant Professor; and from 1999 to 2011, he was an Associate Professor. Since 2011, he has been a Professor with the Department of Electrical and Computer Engineering, Shinshu University. His research interests include linear motors, linear actuators, and electromagnetic sensors. He is a member of the Magnetics Society of Japan and the Japan Society of Applied Electromagnetics and Mechanics (JSAEM).